SPACEBORNE IMAGING RADAR RESEARCH IN THE 90'S

Charles Elachi
Jet Propulsion Laboratory
California Institute of Technology
Pasadena, California

The imaging radar experiments on Seasat (1978) and on the space shuttle (SIR-A in 1981 and SIR-B in 1984) have led to a wide interest in the use of spaceborne imaging radars in Earth and planetary sciences. The radar sensors provide unique and complimentary information to what is acquired with visible and infrared imagers. This includes subsurface imaging in arid regions (1,2), all weather observation of ocean surface dynamic phenomena (3-5), structural mapping (6-8), soil moisture mapping (9), stereo imaging and resulting topographic mapping (10).

However, experiments up to now have exploited only a very limited range of the generic capability of radar sensors. With planned sensor developments in the late 80's and early 90's, a quantum jump will be made in our ability to fully exploit the potential of these sensors. These developments include (Figure 1): multiparameter research sensors such as SIR-C and X-SAR, long-term and global monitoring sensors such as ERS-1, JERS-1, EOS, Radarsat, GLORI and the spaceborne sounder, planetary mapping sensors such as the Magellan and Cassini/Titan mappers, topographic three-dimensinal imagers such as the scanning radar altimeter and three-dimensional rain mapping. These sensors and their associated research are briefly described in this paper.

I. MULTIPARAMETER RESEARCH IMAGING RADAR. THE SIR PROJECT

An evolutionary ten-year program is ongoing at NASA's Jet Propulsion Laboratory to develop the scientific application and technological aspects of multiparameter imaging radars. The first two steps consisted of the SIR-A, which was a single-frequency proof of concept sensor, and the SIR-B, which was designed to acquire multiangle imagery. The SIR-A demonstrated the ability of spaceborne radars to acquire subsurface imagery in arid regions (Figure 2). The SIR-B provided for the first time stereo and three-dimensional imagery from space (Figure 3). For recent results acquired with SIR-B the reader is referred to references 10 and 11.

The next major step is the joint US/Germany/Italy SIR-C/X-SAR experiment which will allow the simultaneous acquisition of images at three frequencies (L, C and X) and at all polarization states (on the L and C channels). The multifrequency capability will allow the study of the surface spectral response and the classification of surface units based on the roughness and dielectric properties. In addition, it will allow the quantitative determination of the subsurface penetration which is a strong factor of the frequency.

The polarization capability will allow the synthesis of the surface images at each and every possible polarization state based on acquiring coherently the four fundamentals (HH, VV, HV, and VH) as shown in Figure 4 and discussed in detail in recent publications (12-14).

The SIR project activities also include major technological developments (distributed SAR, real-time ground data processing and calibration) which will form the basis for the EOS SAR.

II. LONG-TERM AND GLOBAL OBSERVATIONS

The SIR experiment will be limited to short-period flights (1 week) until the EOS platform is put in orbit in the mid-90's. In the mean time, a number of imaging radar sensors are planned for launch on free flyers in the early 90's for long-term surface observation. These sensors will have limited parameter flexibility, but will play a major role in allowing the study of temporal behavior of surface phenomena such as sea ice, ocean waves and patterns, vegetation dynamics, forest clear cutting, etc... The European ERS-1 and Japanese ERS are approved projects that are planned for the early 90's with a lifetime of 2 to 3 years. However, because of their limited swath (100 km) and limited operation range (in view of a station) their monitoring capability will be localized. This led JPL scientists to the feasibility study of a Global Radar Imager (GLORI) which will allow global mapping every two days. This requires a sensor with dual 400-km swaths. Preliminary considerations correspond to a C-band sensor with a 100-m resolution and real-time processing on the EOS platform. Such a sensor will allow global and continuous monitoring of polar ice, large ocean phenomena (internal waves, eddies, weather fronts, current boundaries), soil moisture and vegetation cover.

Subsurface penetration is directly proportional to the observing radar wavelength. This led to the considerations of a low-frequency imaging SAR. Even though very low frequencies are desired, ionospheric efforts and frequency allocation considerations will limit the lower range to no less than about 400 MHz. This would extend the penetration depth in arid regions observed by SIR-A by a factor of 3. In addition, such a sensor would allow the sounding of the antarctic ice sheets down to a depth of many kilometers due to the extremely low loss of sheets of ice.

III. PLANETARY OBSERVATIONS

The cloud penetration capability of radar sensors makes it necessary to use them to image the surfaces of Venus and Titan, which are continuously and completely cloud covered. The Magellan mission will put an S-band imaging SAR in orbit around Venus in 1990, which will provide images of at least 90% of the planet's surface at a resolution better than 250 meters. By the late 90's the Cassini spacecraft will be put in an orbit around Saturn and, through a series of flybys, the surface of Titan will be imaged and sounded with a dual-frequency (L-band and K-band) imaging radar sensor.

IV. THREE-DIMENSIONAL IMAGING

The surface topography is the key data base that is necessary to fully interpret the imaging data acquired with multispectral (microwave, infrared and visible) sensors. When the topography is registered to the imaging data, the interpreter can use graphic techniques to observe the surface from a variety of perspective views (Figure 6), thus enhancing his interpretation capability.

High-resolution topography can be derived from stereoimagery (radar or visible/IR). However, this is practical only for regional coverage. The acquisition of a global digital data base at a reasonable cost and in a timely fashion requires the development of a direct technique which allows the direct measurement of the surface topography in a digital format. This can be done with a scanning radar altimeter (SRA) as shown in Figure 5.

The SRA uses a narrow beam antenna across the track with a surface footprint of 250 meters. This is possible with an 8-meter, 37-GHz antenna from an altitude of 250 km. Along the track, a synthetic-aperture technique is used to achieve the equivalent spatial resolution. This requires an antenna of only 0.3 meter. The beam is scanned back and forth across the track to cover a 150-km swath. In this configuration, two shuttle flights will be sufficient to acquire the global data sets. Height accuracy measurement of less than 3 meters is easily feasible.

The scanning radar altimeter concept can also be used for volumetric rain mapping. Figure 7 shows an example of rain profiles acquired with a down-looking airborne sensor (13). The rain intensity can be derived for each altitude level particularly if a dual-frequency sensor is used. By scanning back and forth, a three-dimensional "picture" of the rain region can be acquired.

V. CONCLUSION

The above overview illustrates the wide range of experiments that are planned to fully capitalize on the capability of spaceborne radar sensors. It is important to note that in order to acquire a comprehensive information set about the surface, the radar data has to be used in conjunction with visible and infrared data. In this fashion the user will be able to determine the surface composition (from visible and infrared spectrometry), its thermal properties (from thermal infrared), its physical and electric properties (from multispectral imaging radar) and its morphology (from stereo imagers or scanning altimeters).

REFERENCES

1. McCauley, J. et al. (1982), "Subsurface valleys and geoarcheology in the eastern Sahara revealed by shuttle radar," Science, vol. 218, p. 1004.

2. Elachi, C., L. Roth and G. Schaber (1984), "Spaceborne radar subsurface imaging in hyperarid regions," IEEE Trans. G&RS, vol. GE-22, p. 383. Note: The SIR-A and Landsat images in Fig. 2 were mistakenly interchanged.

3. Vesecky, J. and R. Stewart (1982), "The observation of ocean surface phenomena using imagery from Seasat SAR," JGR, vol. 87 (C3), p. 3397.

4. Elachi, C. (1980), "Spaceborne imaging radar: geologic and oceanographic applications," Science, vol. 209, p. 1073.

5. Elachi, C. (1978), "Radar imaging of the ocean surface," Boundary Layer Meteorology, vol. 13, p. 165.

6. Sabins Jr., F. F. (1983), "Geologic interpretation of space shuttle radar images of Indonesia," AAPG, vol. 67, p. 2076.

7. Ford, J. P. (1980), "Seasat orbital radar imagery for geologic mapping: Tennessee-Kentucky-Virginia," AAPG, vol. 66, p. 2064.

8. Sabins Jr., F. F., R. Blom and C. Elachi (1980), "Seasat radar image of the San Andreas Fault, California," AAPG, vol. 64, p. 614.

9. Carver, K., C. Elachi and F. Ulaby (1986), "Microwave Remote Sensing," IEEE Proc., vol. 73, p. 970.

10. See Science Issue of June 20, 1986, vol. 232.

11. Cimino, J. B., C. Elachi and M. Settle (1986), "SIR-B – The second shuttle imaging radar experiment," IEEE Trans. G&RS, vol. GE-24, p. 445.

12. Evans, D., T. Farr, J. P. Ford, T. Thompson, C. Werner (1986), "Multi-polarization radar images for geologic mapping and vegetation discrimination," IEEE Trans. G&RS, vol. GE-24, p. 246.

13. Van Zyl, J., H. Zebker and C. Elachi, "Theory of imaging radar polarimetry through wave synthesis," submitted to Radio Science, 1986.

14. Zebker, H., J. van Zyl and D. Held, "Imaging radar polarimetry from wave synthesis," submitted to Journal for Geophysical Research, 1986.
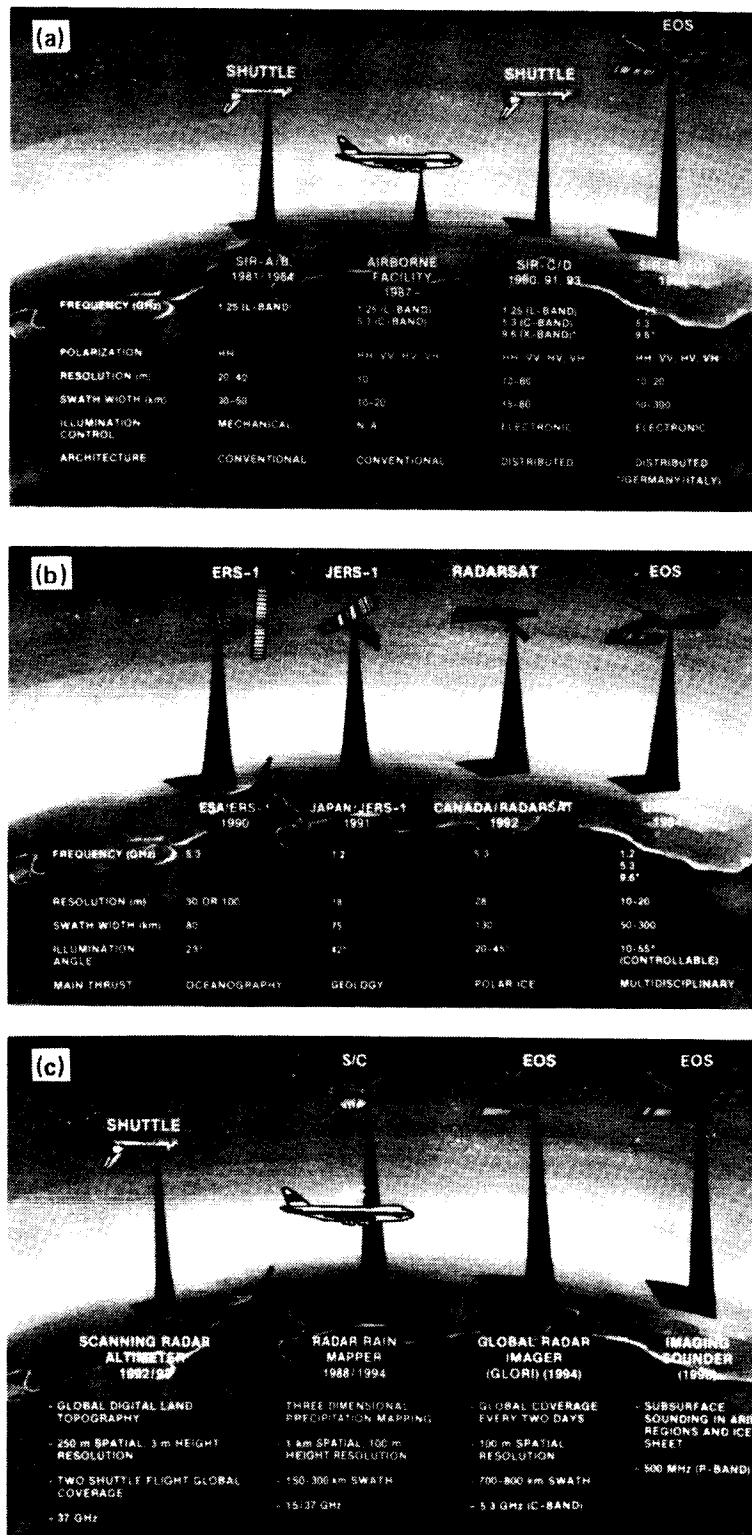
Figure 1. Spaceborne imaging radar sensors of the 80's and 90's:
a) Completed and ongoing elements of the NASA SIR core
project; b) International free flying sensors; c) non-
conventional spaceborne imaging radar sensors being
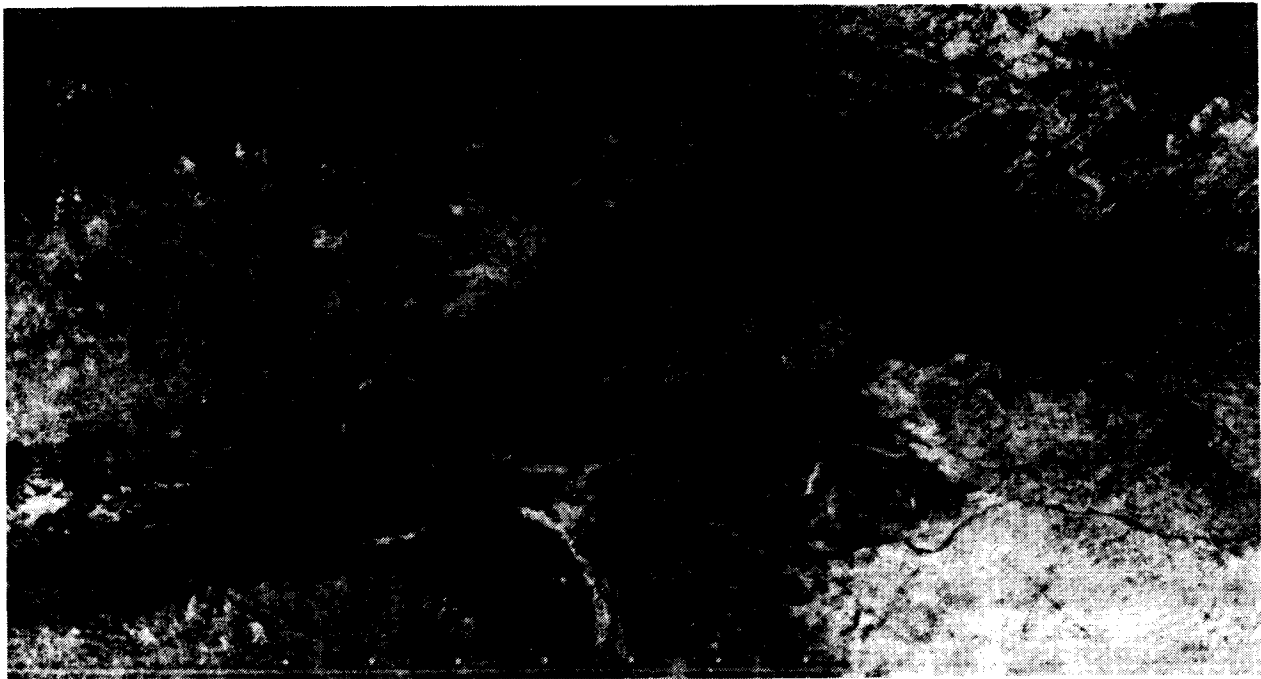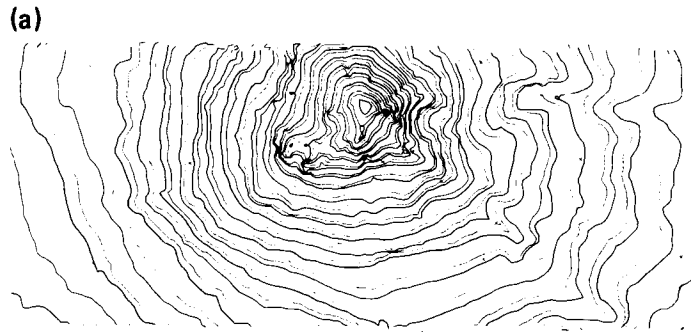studied.

49

20 km

Figure 2. SIR-A and Landsat images of the same desert area in southwestern
Egypt. The SIR-A image (bottom) clearly shows the morphology of
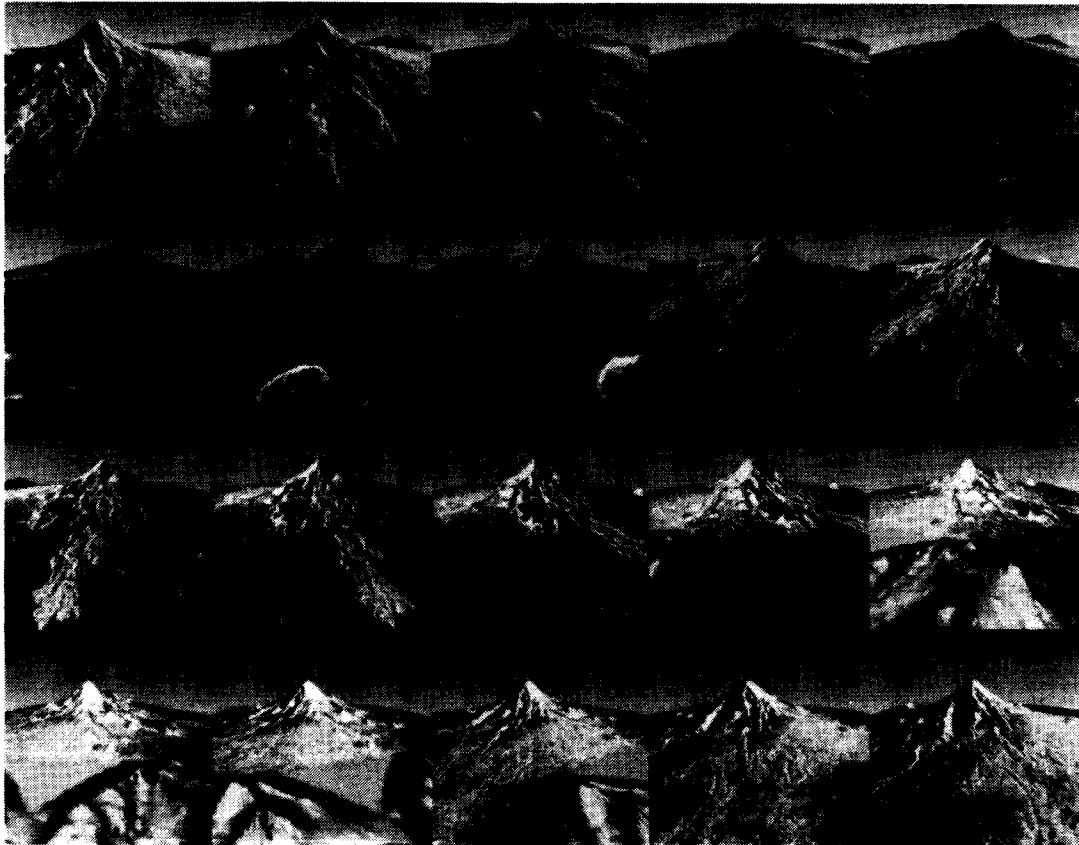dry river channels buried a few meters under a layer of dry sand.

(a)

(b)

Figure 3. Stereo images acquired by SIR-B were used to generate (a) topo-
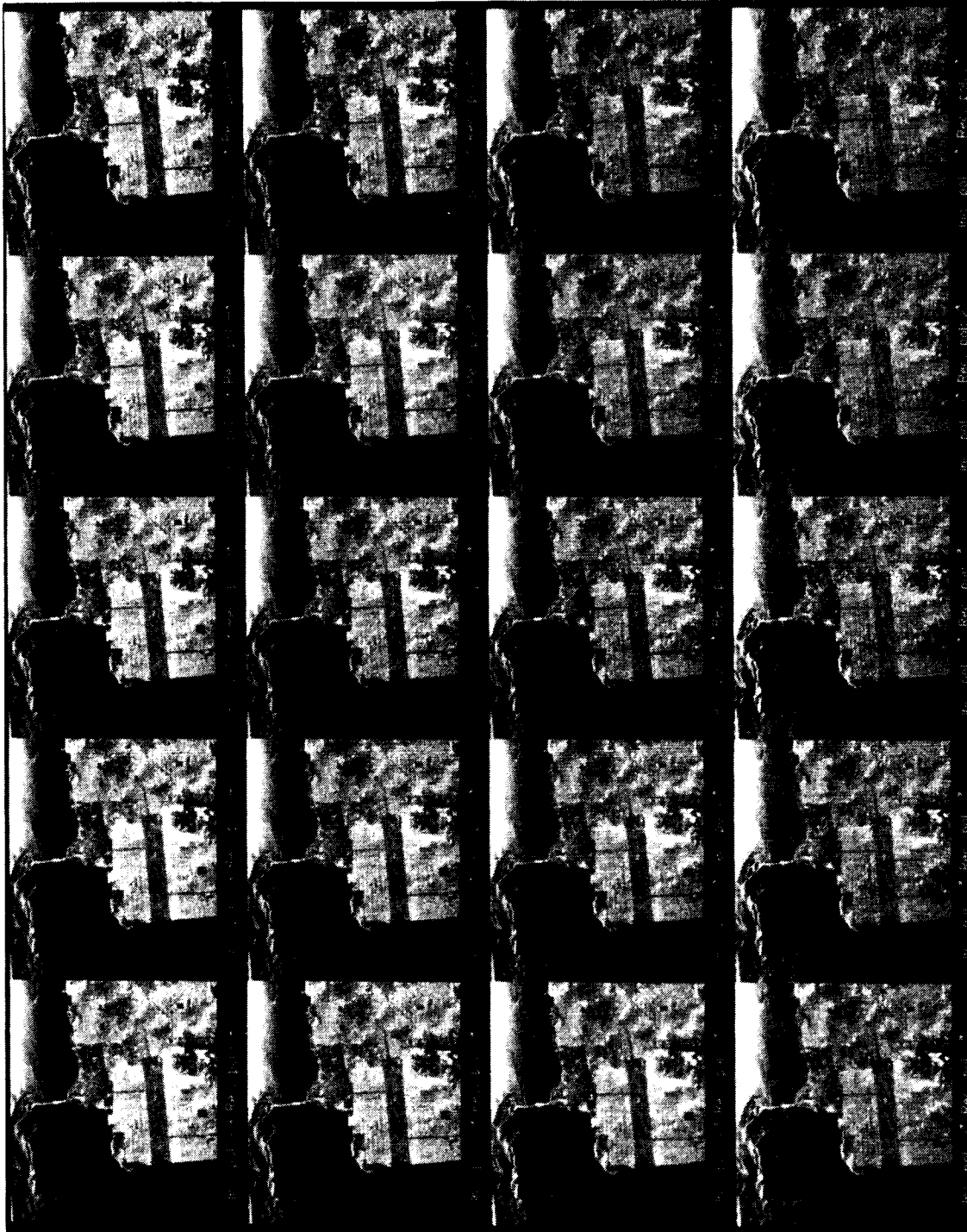graphic contours and (b) perspective views of Mt. Shasta,
California.

51

Figure 4. Synthesized polarization diversity images of San Francisco Bay generated from the four basic coherent images at HH, VV, VH, and HV polarization acquired with the JPL L-band airborne radar.
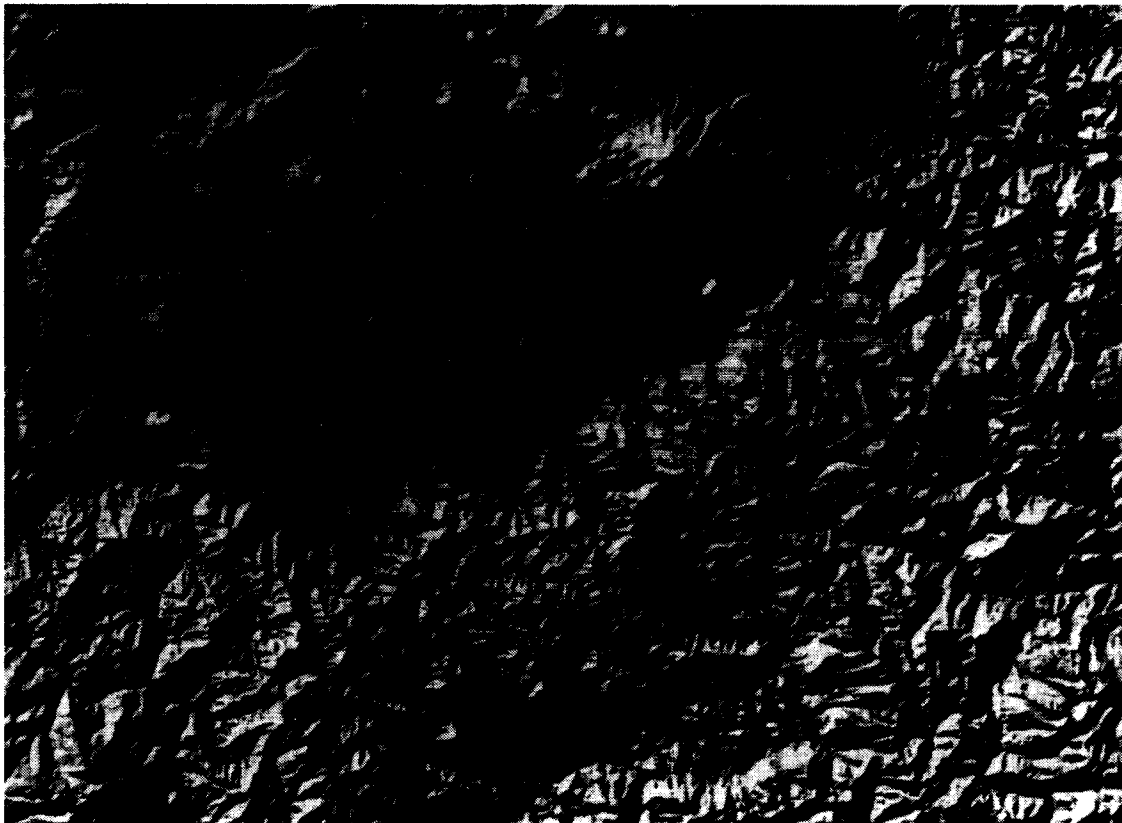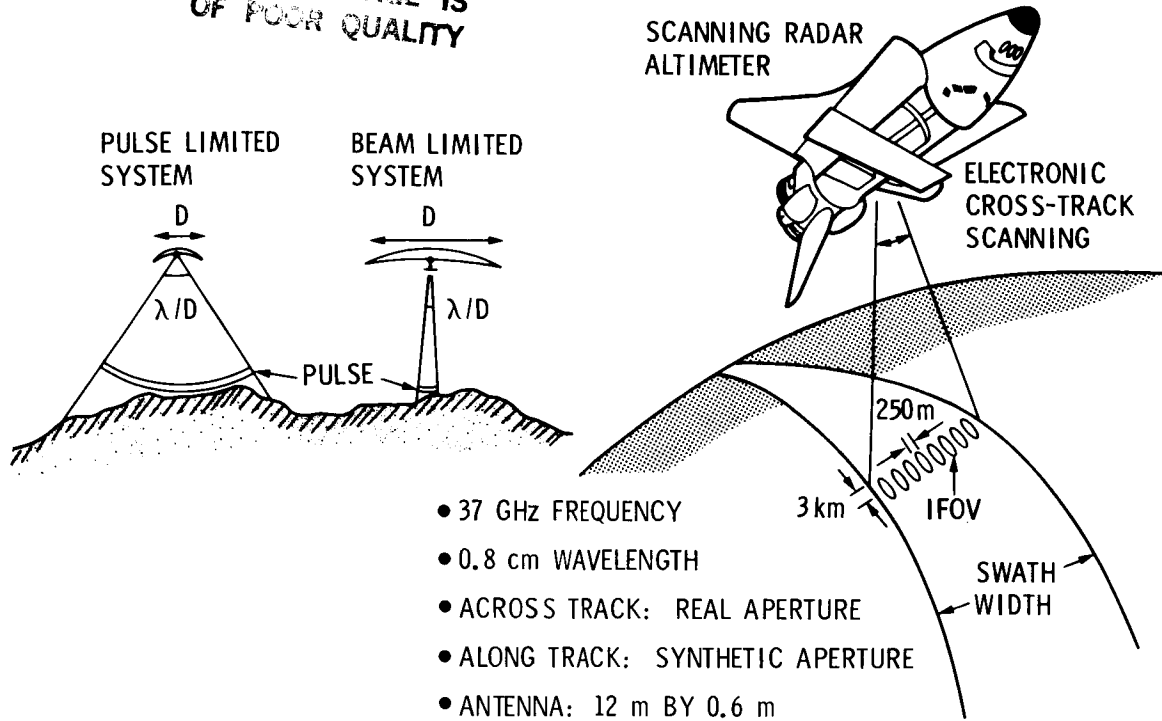
PULSE LIMITED
SYSTEM

BEAM LIMITED
SYSTEM

SCANNING RADAR
ALTIMETER

ELECTRONIC
CROSS-TRACK
SCANNING

PULSE

250 m

3 km   IFOV

SWATH
WIDTH

- 37 GHz FREQUENCY
- 0.8 cm WAVELENGTH
- ACROSS TRACK: REAL APERTURE
- ALONG TRACK: SYNTHETIC APERTURE
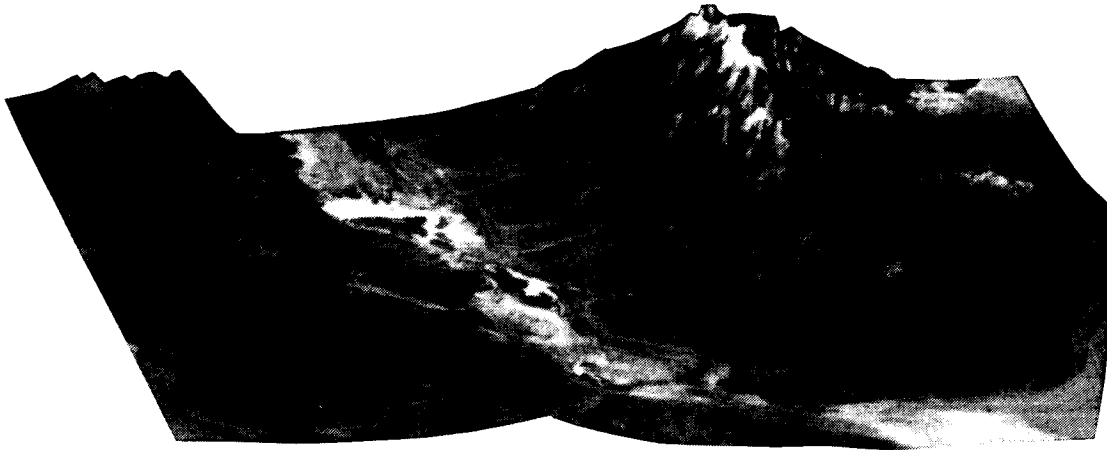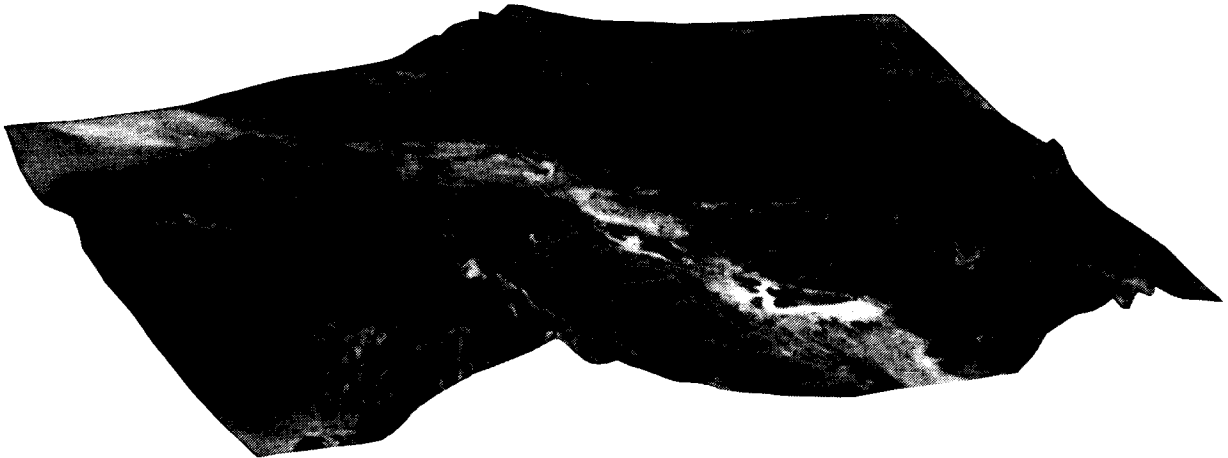- ANTENNA: 12 m BY 0.6 m

Figure 5.   Concept of a scanning imaging altimeter for global topographic
mapping and a shaded relief map of Mt. Shasta generated from a
simulation of the data that will be provided by such a sensor.

53

DEATH VALLEY FROM NORTHEAST – TM BAND 1

DEATH VALLEY FROM SOUTHEAST – TM BAND 1

Figure 6. Perspective views of Death Valley, California, generated from thematic mapper data coregistered on a digital surface topography base.
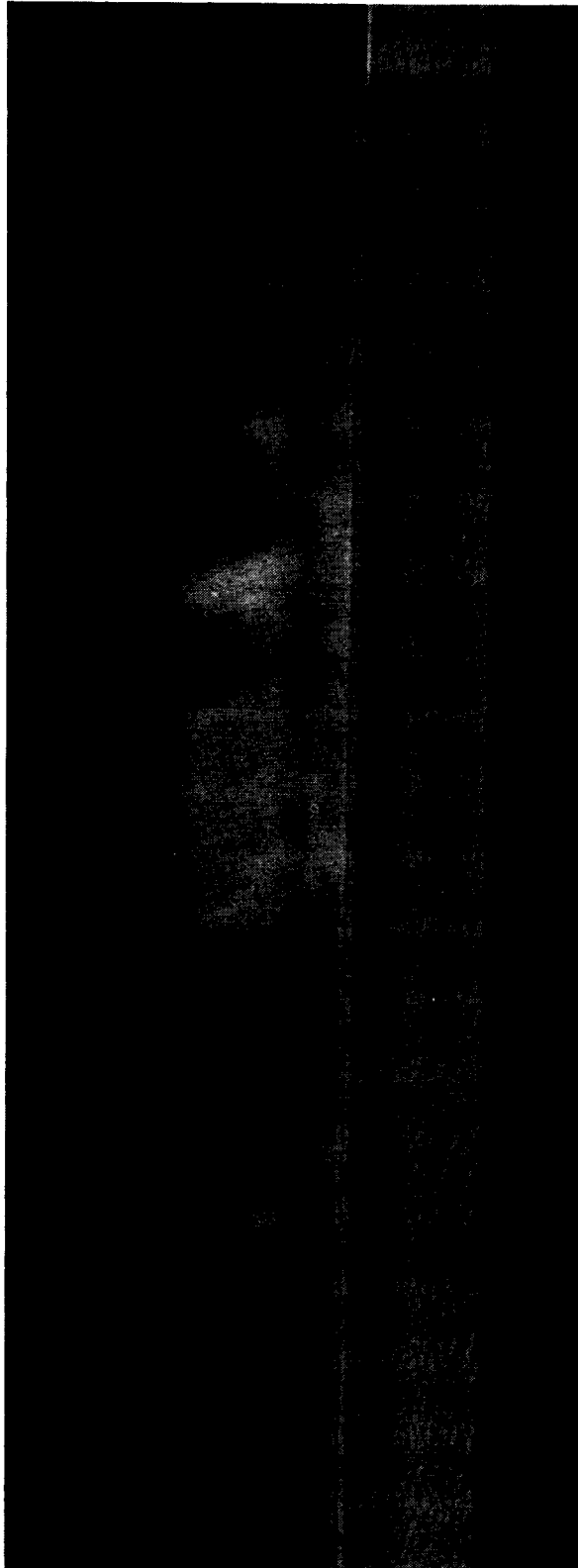
54

Figure 7. Concept of a scanning radar rain mapper and example of airborne radar data showing rain images in one vertical plane.